

Swift/BAT monitoring of Fermi/LAT sources

Hans A. Krimm

CRESST, Universities Space Research Association and NASA GSFC, Greenbelt, MD 20771, USA

Scott D. Barthelmy, Neil Gehrels, Jack Tueller
NASA Goddard Space Flight Center, Greenbelt, MD 20771, USA

Wayne H. Baumgartner, Jay R. Cummings, Taka Sakamoto
CRESST, University of Maryland, Baltimore County and NASA GSFC, Greenbelt, MD 20771, USA

Edward E. Fenimore, David M. Palmer
Los Alamos National Laboratory, P.O. Box 1663, Los Alamos, NM 87545, USA

Craig B. Markwardt, Gerald K. Skinner
CRESST, University of Maryland, College Park and NASA GSFC, Greenbelt, MD 20771, USA

Michael Stamatikos
NASA Goddard Space Flight Center and Ohio State University, Columbus, OH 43210, USA

The Swift Burst Alert Telescope (BAT) hard X-ray transient monitor tracks more than 700 galactic and extragalactic sources on time scales ranging from a single Swift pointing (approximately 20 minutes) to one day. The monitored sources include all objects from the Fermi LAT bright source list which are either identified or which have a 95% error confidence radius of less than eight arc minutes. We report on the detection statistics of these sources in the BAT monitor both before and after the launch of Fermi.

I. THE SWIFT/BAT HARD X-RAY SURVEY

The *Swift*/BAT Hard X-ray Survey [3, 4] uses the full *Swift*/BAT data in eight energy ranges (covering 14-195 keV) to produce a map (mosaic) of the full sky. The primary goal of the BAT Survey is to make a complete census of nearby AGN down to a 4.8σ sensitivity of $2.2 \times 10^{-11} \text{ erg cm}^{-2} \text{ s}^{-1}$ (1 mCrab). The current published results cover the first 22 months of the *Swift* mission from December 2004 through September 2006. The data used in this paper cover the first 36 months (through November 2007) and processing is underway to complete the full 60 months of the mission to date. Although sources are only announced if they are at least 4.8σ , we have used the sky maps to search for lower level emission from the 175 sources in the LAT Bright Source list which are included in the BAT Monitor catalog. Other work which correlates BAT and LAT blazar detections has been done by Sambruna et al (in preparation) who have used BAT and LAT spectral fits to argue in favor of the “blazar sequence” relating the X-ray and γ -ray continua.

II. SUMMARY OF RESULTS

- Using a low threshold, we find that BAT can detect 31 of the 108 identified blazars in the LAT Bright Source Catalog and 18 other sources

- Given the significance distribution, we expect that many more blazars will be detected as the BAT Survey and Monitor become more sensitive
- Preliminary blazar SEDs in the *Swift* energy range are consistent with the standard models of FSRQ and BL Lac blazar types

III. DISTRIBUTION OF BAT SIGNIFICANCES

The histograms in Figure 1 are derived from the *Swift*/BAT Hard X-ray Transient Monitor (top) and *Swift*/BAT Hard X-ray Survey (bottom). The plots on the left show sources in the first *Fermi*/LAT Bright Source List and the plots on the right show sources from 106 “blank sky” points in the Transient Monitor catalog. The blank sky points are distributed randomly across the sky and each point has been checked against all of the X-ray catalogs in Simbad (<http://simbad.u-strasbg.fr/simbad/sim-fid>) to ensure that there is no hard or soft X-ray source nearby.

To create the Transient Monitor histograms, we have calculated the mean daily average count rate for each source and divided by the mean count rate for a source one thousandth the rate of the Crab ($2.22 \times 10^{-4} \text{ ct cm}^{-2} \text{ s}^{-1}$). The histograms are color-coded for source type, with black representing the sum of the three categories. For non-detections, these

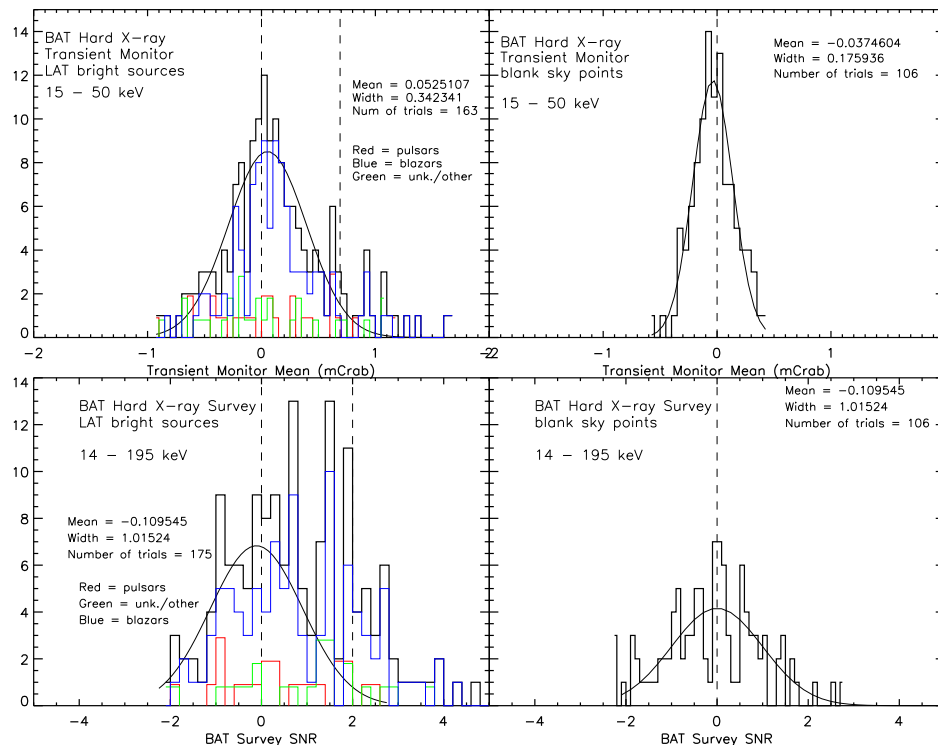


FIG. 1: Histograms of count rates and signal-to-noise ratios (SNR) for *Fermi*/LAT bright sources from the *Swift*/BAT Hard X-ray Transient Monitor and Hard X-ray Survey. **Top Left:** Histogram of the average count rate derived for each *Fermi*/LAT bright source in the BAT Transient Monitor. Note the asymmetry in the distribution. The dashed vertical line to the right indicates the detection threshold of 2σ . **Top Right:** A similar distribution for “blank sky” points in the monitor catalog. The distribution is narrower than the one on the left because these sources were monitored for a longer period. **Bottom Left:** A distribution of SNR from the BAT Survey, again showing a pronounced positive excess. **Bottom Right:** The distribution for the blank sky points shows no such asymmetry.

means are centered on zero (top right of Fig 1). By contrast, for the LAT bright sources, there is a strong bias toward the positive side, telling us that a high percentage of these sources are detected. In the top left of Fig 1 there are 35 sources at $> 2\sigma$ (including 12 off the plot to the right), compared to 4 expected. This enables us to set a low detection threshold, as indicated by the dashed vertical line to the right, corresponding to 0.68 mCrab. The width of the blank sky distribution is smaller than that of the *Fermi* bright sources for the following reason. Light curves for the blank sky points have been accumulated since near the start of the *Swift* mission (57 months since Feb. 2005), while light curves for most of the LAT sources have only been accumulated for only 9 months since the release of the first LAT bright source catalog. Thus the distribution of means is tighter.

A similar pair of histograms are created from the results of the 36-month *Swift*/BAT Hard X-ray Survey[5]. In these plots, the histograms are based on the signal-to-noise ratio (SNR) for each source. Therefore, the blank-sky histogram has a mean near

zero and width near unity. The fit to the blank-sky histogram is overlaid on the bright-source histogram. For the survey, with a sensitivity about twice that of the monitor (due mostly to the longer collection time), we see an even greater asymmetry to the positive side. This suggests that a large number of the LAT blazars are in fact detected in the BAT and that many more will be detected as the Survey and Monitor run longer and become more sensitive. The dashed vertical line to the right indicates 2σ .

IV. RELATION OF BAT AND LAT FLUXES

Figure 2 shows that there is little or no correlation between the LAT 100 MeV to 1 GeV flux and the BAT 15-50 keV rate. This is not surprising, since the relationship between these two quantities depends strongly on where the peak lies in the spectral energy distribution for each blazar. A few points can be gleaned from this figure. First of all, most of the BAT-detected BL Lacs (such as Mrk 421 and Mrk 501) are

relatively faint in the LAT, while BAT tends to detect more of the brighter LAT flat-spectrum radio quasars. Also, none of the unknown type blazars are detected in the BAT.

V. SPECTRAL ENERGY DISTRIBUTIONS

For 27 of the BAT-detected blazars, we have produced preliminary spectral energy distributions (SED) in the energy ranges of *Swift* XRT and BAT. The XRT points were taken from a single *Swift* observation (the one with the longest exposure time) and the unabsorbed flux and photon index were derived using the web interface developed by Phil Evans at the UK Swift Science Data Centre at the University of Leicester[1, 2]. For four blazars (PKS 1830-211, PKS 0142-278, B3 2322+396 and PKS 2023-07) there were either no XRT observations in the archive or we were unable to adequately fit the spectrum. The BAT SED points were derived using WebPIMMS (<http://heasarc.gsfc.nasa.gov/Tools/w3pimms.html>) to convert from the BAT average 14-195 keV count rate to the flux density at 100 keV. Thus Fig 3 does mix an XRT point at a single time with a mean BAT point. Given the variations in blazar outputs, a more proper analysis (see Future Work) will include, where possible, more closely coincident spectral analysis.

For most flat-spectrum radio quasars (FSRQs), BAT appears to be on the rising part of the Compton peak, though for the brightest two (3C 273 and 3C 454.3), BAT is near the top of Compton peak. For several of the high-frequency peaked BL Lacs (Mrk 421, Mrk 501, QSO B0033+595), the BAT appears to be on the falling edge of the synchrotron peak. For others the dip in the SED is apparently below the BAT energy range, so the BAT points are again on the rising part of the Compton peak.

VI. FUTURE WORK

- Re-run the BAT Transient Monitor to get complete light curves for all LAT bright sources back to the start of the *Swift* mission
- Derive BAT spectral fits from the 8-channel BAT Survey results

- Look for source time variability and either derive time-integrated XRT spectral fits or time-resolved BAT spectral fits
- Look for temporal BAT-LAT correlations for the brightest BAT sources
- Further study individual blazars and relate BAT results to what is known about particular sources and source classes.

VII. DATA TABLES

The BAT results are shown in two tables. In Table I, we list the 49 LAT sources which are detected in either the BAT monitor or BAT survey with the criteria that *either* the source is seen at at least 0.64 mCrab in the BAT Transient Monitor or at $> 3\sigma$ in the BAT Survey. The common name and the source name in the *Fermi*/LAT Bright Source List are listed, along with the source type from the LAT[6]. The results from the BAT Monitor are given in mCrab and from the BAT Survey in SNR. The XRT flux and photon index were derived for the blazars (see Section V for details).

For two sources (noted with an asterisk), the LAT identification is with a region of the sky that contains the source listed: the Galactic Center region for Sgr A* and the Large Magellanic Cloud for LMC X-1. The BAT results are given for the individual sources, although there is still confusion at the BAT resolution for the Galactic Center.

One pulsar (PSR J2124-3358) and three of the four unidentified LAT sources in the table have BAT Survey SNR < 0 , but a possible detection in the BAT Monitor. This tells us that these sources are probably variable in the hard X rays, which is suggestive of their being galactic transient sources.

Table II shows the 20 brightest LAT sources overall and the 20 brightest blazars. BAT-detected sources are indicated in bold and undetected sources in italics. The LAT fluxes in the two bands are scaled to the average flux in each band and the rankings are based on the 100 MeV to 1 GeV flux. Only about half of the brightest LAT blazars are detected in the BAT, although most of the sources in the list have BAT Survey significance above 1.7σ , so are likely to be detected in a deeper survey.

[1] Evans, P. A. et al, MNRAS, submitted, arXiv:0812.3662

[2] http://www.swift.ac.uk/user_objects.

[3] Tueller, J. et al, 2009, arXiv0903.3037

[4] <http://swift.gsfc.nasa.gov/docs/swift/results/bs22mon/>

[5] Tueller, J. et al, 2010, in preparation

[6] PSR=pulsar; rdg=radio galaxy; bzq=FSRQ blazar; bzb=BL Lac; x=special case; HXB=high-mass X-ray binary; NONE=no type listed in LAT source list

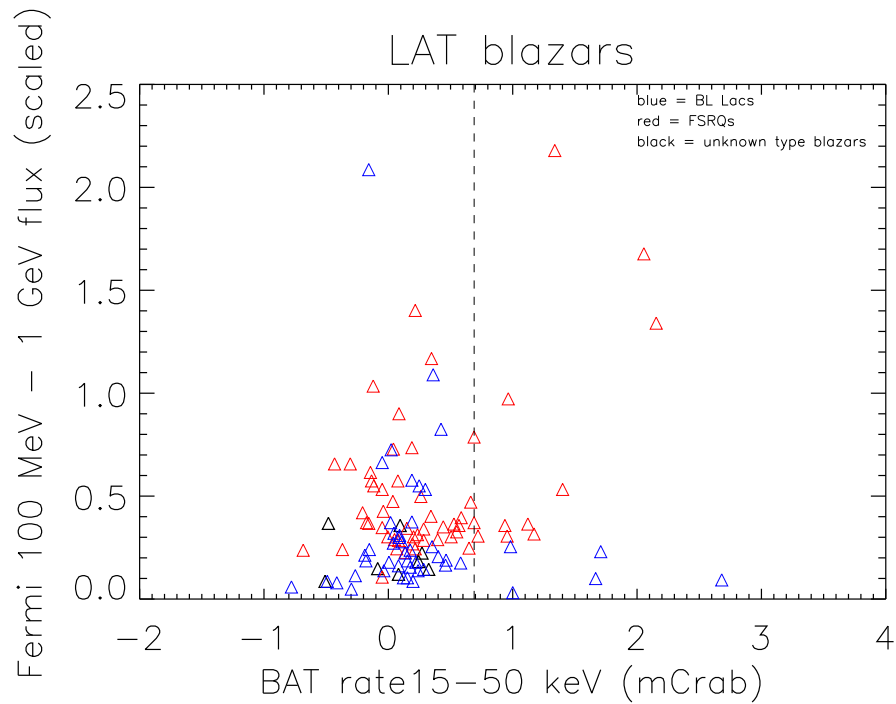


FIG. 2: The Fermi flux (scaled to the mean flux) in the 100 MeV - 1 GeV band is plotted relative to the BAT Monitor count rate in mCrab. The vertical line indicates our BAT detection threshold. We see no apparent correlation here, which is not surprising, given that the relationship between BAT and LAT flux depends strongly on where the peaks in the spectral energy distributions lie.

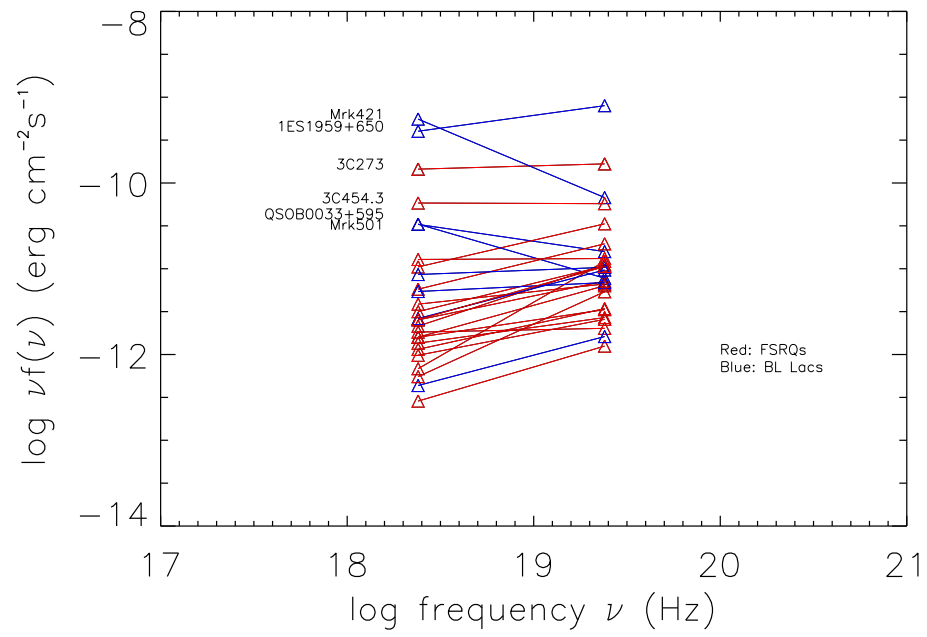


FIG. 3: Preliminary spectral energy distributions (SED) for BAT-detected blazars based on BAT and XRT observations.

TABLE I: Swift/BAT detections of Fermi/LAT bright sources

Name	Fermi name	Type	BAT monitor mCrab	BAT survey SNR	XRT flux $erg\ cm^{-2}\ s^{-1}$	XRT photon index
Crab	J0534.6+2201	PSR	1000.00	4605.02	–	–
Cen A	J1325.4-4303	rdg	46.27	194.37	–	–
3C 273	J1229.1+0202	bzq	11.28	101.78	2.90×10^{-10}	1.64
* Sgr Astar	J1746.0-2900	NONE	7.79	32.87	–	–
Vela Pulsar	J0835.4-4510	PSR	5.73	45.46	–	–
Mrk 421	J1104.5+3811	bzb	5.71	60.09	1.40×10^{-09}	1.80
NGC 1275	J0320.0+4131	rdg	4.51	30.88	–	–
3C 454.3	J2254.0+1609	bzq	3.82	30.70	9.00×10^{-11}	1.44
Mrk 501	J1653.9+3946	bzb	2.68	16.23	1.40×10^{-10}	2.11
* LMC X-1	J0538.4-6856	NONE	2.42	10.70	–	–
PKS 1830-211	J1833.4-2106	bzq	2.15	9.98	–	–
QSO J1512-0906	J1512.7-0905	bzq	2.05	9.08	1.20×10^{-11}	1.17
QSO B0033+595	J0036.7+5951	bzb	1.71	8.67	1.30×10^{-10}	2.06
1ES 1959+650	J2000.2+6506	bzb	1.67	13.41	3.50×10^{-10}	2.46
PKS 2325+093	J2327.3+0947	bzq	1.40	6.05	3.50×10^{-12}	1.49
QSO B1502+1041	J1504.4+1030	bzq	1.34	5.53	1.00×10^{-12}	1.40
PSR J1418-60	J1418.8-6058	PSR	1.21	2.52	–	–
PKS 0142-278	J0145.1-2728	bzq	1.17	2.99	–	–
0FGL J1830.3+0617	J1830.3+0617	NONE	1.14	-0.56	–	–
RX J1826.2-1450	J1826.3-1451	hxb	1.14	3.86	–	–
QSO J1130-1449	J1129.8-1443	bzq	1.12	11.04	1.00×10^{-11}	1.54
B3 2322+396	J2325.3+3959	bzb	1.00	0.87	–	–
QSO B2200+420	J2202.4+4217	bzb	0.98	8.09	2.90×10^{-11}	1.98
0FGL J1834.4-0841	J1834.4-0841	x	0.96	1.52	–	–
3C 279	J1256.1-0547	bzq	0.96	8.03	1.60×10^{-11}	1.75
PMN J0948+0022	J0948.3+0019	bzq	0.96	1.38	3.80×10^{-12}	1.67
PKS 1329-049	J1331.7-0506	bzq	0.94	4.19	3.40×10^{-12}	1.69
PSR J1826-1256	J1825.9-1256	PSR	0.88	0.79	–	–
2CG 135+01	J0240.3+6113	HXB	0.77	9.88	–	–
0FGL J1231.5-1410	J1231.5-1410	NONE	0.76	-0.44	–	–
PSR J2124-3358	J2124.7-3358	PSR	0.75	-0.42	–	–
QSO J0217+0144	J0217.8+0146	bzq	0.72	2.11	3.30×10^{-12}	1.67
0FGL J1413.1-6203	J1413.1-6203	NONE	0.71	-1.58	–	–
PKS 0528+134	J0531.0+1331	bzq	0.69	2.84	7.30×10^{-12}	1.60
4C 11.69	J2232.4+1141	bzq	0.69	6.66	6.60×10^{-12}	1.67
PSR J1509-5850	J1509.5-5848	PSR	0.68	0.81	–	–
PSR J1809-2332	J1809.5-2331	PSR	0.67	0.88	–	–
PSR B1706-44	J1709.7-4428	PSR	0.67	2.45	–	–
PKS 0227-369	J0229.5-3640	bzq	0.66	1.75	1.60×10^{-12}	1.49
PKS 1244-255	J1246.6-2544	bzq	0.65	1.65	2.50×10^{-12}	2.46
QSO B2052-474	J2056.1-4715	bzq	0.57	3.45	4.90×10^{-12}	1.62
QSO B0917+449	J0921.2+4437	bzq	0.50	3.05	5.10×10^{-12}	2.04
QSO B1514-241	J1517.9-2423	bzb	0.46	4.51	5.70×10^{-12}	1.70
QSO B0537-441	J0538.8-4403	bzb	0.36	5.73	1.40×10^{-11}	1.82
QSO B2227-0848	J2229.8-0829	bzq	0.34	4.85	4.50×10^{-12}	1.55
QSO B0716+714	J0722.0+7120	bzb	0.30	3.60	6.00×10^{-12}	2.66
PKS 2023-07	J2025.6-0736	bzq	0.22	4.01	–	–
QSO B2201+1711	J2203.2+1731	bzq	0.19	3.13	1.10×10^{-12}	1.64
8C 1849+670	J1849.4+6706	bzq	0.04	3.27	3.50×10^{-12}	1.92

TABLE II: The Brightest Fermi/LAT bright sources

Name	Fermi name	Type	LAT Flux (scaled) (100 MeV – 1 GeV)	LAT flux (scaled) 1 GeV – 100 GeV	BAT survey SNR
Overall Brightest sources					
Vela Pulsar	J0835.4-4510	PSR	27.60	42.35	45.46
<i>Geminga</i>	<i>J0634.0+1745</i>	<i>PSR</i>	<i>9.84</i>	<i>23.28</i>	<i>0.97</i>
3C 454.3	J2254.0+1609	bzq	7.28	3.71	30.70
Crab	J0534.6+2201	PSR	7.01	5.82	4605.02
<i>PSR J2021+4026</i>	<i>J2021.5+4026</i>	<i>PSR</i>	<i>4.25</i>	<i>4.00</i>	<i>-1.00</i>
Sgr Astar	J1746.0-2900	NONE	4.03	2.99	32.87
PSR B1706-44	J1709.7-4428	PSR	3.96	5.98	2.45
PSR J1826-1256	J1825.9-1256	PSR	3.27	2.18	0.79
<i>0FGL J1855.9+0126</i>	<i>J1855.9+0126</i>	<i>x</i>	<i>3.06</i>	<i>2.62</i>	<i>0.80</i>
<i>0FGL J1801.6-2327</i>	<i>J1801.6-2327</i>	<i>x</i>	<i>2.55</i>	<i>1.70</i>	<i>-0.22</i>
<i>PSR J2021+3651</i>	<i>J2020.8+3649</i>	<i>PSR</i>	<i>2.54</i>	<i>2.37</i>	<i>1.41</i>
2CG 135+01	J0240.3+6113	HXB	2.42	1.26	9.88
RX J1826.2-1450	J1826.3-1451	hxb	2.32	0.93	3.86
3C 273	J1229.1+0202	bzq	2.20	0.61	101.78
QSO B1502+1041	J1504.4+1030	bzq	2.18	2.21	5.53
<i>AO 0235+16</i>	<i>J0238.6+1636</i>	<i>bzb</i>	<i>2.09</i>	<i>2.57</i>	<i>1.74</i>
<i>0FGL J1813.5-1248</i>	<i>J1813.5-1248</i>	<i>NONE</i>	<i>1.85</i>	<i>1.05</i>	<i>0.08</i>
<i>0FGL J1839.0-0549</i>	<i>J1839.0-0549</i>	<i>NONE</i>	<i>1.77</i>	<i>1.53</i>	<i>-0.62</i>
<i>PSR J2032+41</i>	<i>J2032.2+4122</i>	<i>PSR</i>	<i>1.76</i>	<i>1.16</i>	<i>1.88</i>
QSO J1512-0906	J1512.7-0905	bzq	1.68	0.70	9.08
Brightest blazars					
3C 454.3	J2254.0+1609	bzq	7.28	3.71	30.70
3C 273	J1229.1+0202	bzq	2.20	0.61	101.78
QSO B1502+1041	J1504.4+1030	bzq	2.18	2.21	5.53
<i>AO 0235+16</i>	<i>J0238.6+1636</i>	<i>bzb</i>	<i>2.09</i>	<i>2.57</i>	<i>1.74</i>
QSO J1512-0906	J1512.7-0905	bzq	1.68	0.70	9.08
PKS 2023-07	J2025.6-0736	bzq	1.40	0.83	4.01
PKS 1830-211	J1833.4-2106	bzq	1.34	0.39	9.98
<i>PKS 0454-234</i>	<i>J0457.1-2325</i>	<i>bzq</i>	<i>1.17</i>	<i>0.99</i>	<i>1.77</i>
QSO B0537-441	J0538.8-4403	bzb	1.09	0.95	5.73
<i>PKS 1454-354</i>	<i>J1457.6-3538</i>	<i>bzq</i>	<i>1.03</i>	<i>0.76</i>	<i>2.11</i>
3C 279	J1256.1-0547	bzq	0.97	0.54	8.03
<i>QSO J0730-116</i>	<i>J0730.4-1142</i>	<i>bzq</i>	<i>0.90</i>	<i>0.66</i>	<i>1.74</i>
<i>3C 66A</i>	<i>J0222.6+4302</i>	<i>bzb</i>	<i>0.82</i>	<i>0.99</i>	<i>2.40</i>
PKS 0528+134	J0531.0+1331	bzq	0.79	0.29	2.84
<i>QSO B0208-5115</i>	<i>J0210.8-5100</i>	<i>bzq</i>	<i>0.74</i>	<i>0.51</i>	<i>1.15</i>
<i>TXS 1520+319</i>	<i>J1522.2+3143</i>	<i>bzq</i>	<i>0.73</i>	<i>0.40</i>	<i>2.15</i>
<i>PKS 0426-380</i>	<i>J0428.7-3755</i>	<i>bzb</i>	<i>0.73</i>	<i>0.75</i>	<i>2.14</i>
<i>PMN J1802-3940</i>	<i>J1802.6-3939</i>	<i>bzb</i>	<i>0.66</i>	<i>0.56</i>	<i>-0.62</i>
<i>B3 0650+453</i>	<i>J0654.3+4513</i>	<i>bzq</i>	<i>0.66</i>	<i>0.48</i>	<i>-0.46</i>
<i>PKS 1622-253</i>	<i>J1625.8-2527</i>	<i>bzq</i>	<i>0.66</i>	<i>0.24</i>	<i>1.59</i>